
STRUCTURAL AND OPTICAL PROPERTIES OF $Cd_{1-x}Zn_xS$ ALLOY QUANTUM DOTS

A. A. ABD EL-RAHMAN ^{(A),*}, F. I. MANDOUH ^(A), M. B. MOHAMMED ^(B), GH. ADEL ^(A), E. A. MAHMOUD^(A),

Faculty of Science, Al-Azhar University, Girl's Branch National Institute of Laser Enhanced Science (NILES), Cairo University. * E-mail: afaf.Abdelmaksoud@gmail.com

ABSTRACT

$Cd_{1-x}Zn_xS$ ($0 \leq x \leq 1$) alloy quantum dots (QDs) were synthesized via coprecipitation method using cetyltrimethyl ammonium bromide (CTAB) as a capping material. Elemental composition of the investigated samples was determined by the energy dispersive x-ray spectroscopy (EDX). X-ray powder diffraction (XRD) and high resolution transmission electron microscope (HRTEM) were used to characterize the crystalline structure, particle size and morphology. XRD analysis indicated that the as synthesized nanomaterials, except for ZnS, have a mixture of cubical and hexagonal phases. The percentage of the hexagonal phase was very small. ZnS nanocrystal has a cubical structure. The particle size and the lattice constant decreased with the increase of Zn content. HRTEM data showed the presence of QDs and confirmed the XRD results. Ultraviolet-visible (UV-vis) absorption spectroscopy was employed to study the optical properties. Absorption band edges showed blue-shift systematically with the increase of Zn content. The results are interpreted in terms of the quantum-size confinement effect. Measurements of XRD and UV-vis absorption spectra under different annealing temperatures up to 400°C were performed. The annealed compositions showed mixture of cubical and hexagonal crystal structure. Tendency for phase transformation, from cubic to hexagonal upon annealing were observed. The degree of tendency for phase transformation increased with the decrease of Zn content and the increase of the annealing temperature. Particle sizes were increased with increasing the annealing temperature. UV- vis absorption spectra exhibited red-shift systematically with the increase of the annealing temperature. The values of the optical band gap energies decreased with increasing annealing temperature.

Keywords: QD; Structural Characterizations; UV-vis spectra; Thermal annealing.

INTRODUCTION

The subject of nanoscale semiconductor particles has been of great interest because of their novel properties and wide-ranged in technological applications. The interest derives from their unique chemical and transport properties which are significantly different from those of the bulk materials as a consequence of the confinement of electrons and the large number of surface atoms [1]. The energy band gap tunability of semiconductor nanoparticles – by changing their constituent stoichiometries- as a function of particle size is one of the most attractive characteristics. This is of critical importance, since one can achieve a wide range of optical and electrical properties from the same substance by only changing its size due to the quantum confinement effect [2].

II–VI chalcogenide semiconducting nanocrystals have attracted attention because they have outstanding potential application due to their high photosensitivity, nonlinear optical and luminescence properties, quantum size ef-

fect and other important chemical and transport properties. Among group II–VI semiconductors, ZnS and CdS are particularly promising candidate because of their applications in solar cells [3], nonlinear optical material [4], luminescent material [1], optoelectronics [5], and as antireflection coating for heterojunction solar cells [6]. Introducing Zn into CdS form CdZnS alloy material, which has direct energy band gap that lies between about 2.4 to 3.7 eV in the bulk state at room temperature [7-8]. Compared with the binary CdS and ZnS, ternary CdZnS is more promising material because of their tunable optical and electrical properties [8-10]. CdZnS alloy nanocrystals show unique composition- dependent properties different from those of their bulk counterpart and from those of binary CdS and ZnS nanocrystal [1, 11-14]. This makes CdZnS suitable material for application as a buffer layer in copper- Indium- Gallium- Selenide based solar cells than CdS, since higher band gap (> 2.4 eV for CdS) will allow more short wavelength photons to reach the absorber layer and generate photocurrent, thus enhancing the efficiency

of the solar cell [15]. CdZnS is also potentially useful as window material for the fabrication of p-n junctions [16], lasers [17] and optical switches [18].

Various methods have been employed to synthesize $Cd_{1-x}Zn_xS$ nanocrystals such as the mechanical alloying [14], precipitate-hydrothermal [11, 19], chemical precipitation [20-21], ultrasonic waves [22], chemical vapor deposition [23], coprecipitation [24], sol-gel processing [25], electrochemical deposition [26] and sputtering [27]. However, these methods are carried out under some special conditions such as isolation of oxygen, high temperature, toxic raw material, complicated equipment for preparation and high cost of equipment operation. Coprecipitation has been known as fast, easy, and large productive method to synthesize nanocrystals in the quantum confinement range. So, in the present work $Cd_{1-x}Zn_xS$ nanoparticles were synthesized using coprecipitation method.

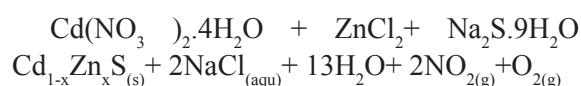
Although many structural and optical properties of $Cd_{1-x}Zn_xS$ nanocrystals have been reported in the literature [11-13], little has been done on the influence of thermal annealing on the structural and optical properties. Bhattacharjee et al [28] have studied the effect of annealing temperature on the structural and optical properties of $Cd_{1-x}Zn_xS$ nanoparticles in thin film form prepared by the sol-gel technique. Knowledge on the influence of thermal annealing on structural and optical properties might be essential in characterizing materials for specific technological application. The present experimental studies were undertaken to (i) provide measurements on the structural and optical properties of $Cd_{1-x}Zn_xS$ ($0 \leq x \leq 1$) alloy QDs at room temperature, (ii) investigate the effect of thermal annealing on the structural properties by the use of XRD, and (iii) study the annealing behaviour of optical properties with increasing annealing temperature.

2. Experimental

2.1 Synthesis of nano- $Cd_{1-x}Zn_xS$ samples

The co-precipitation method was used to prepare the $Cd_{1-x}Zn_xS$ nanomaterials. Cetyltrimethyl ammonium bromide ($(C_{16}H_{33})N(CH_3)_3Br$, PARK- Scientific Limited, 99 %) was used as

a capping material (CTAB). To prepare series of $Cd_{1-x}Zn_xS$ ($0 \leq x \leq 1$) nanoparticles, 1 mmol of Zinc Chloride ($ZnCl_2$) was dissolved in 100 ml of distilled water. Similarly in a separate flask, 1 mmol of Cadmium Nitrate-4-hydrate ($Cd(NO_3)_2 \cdot 4H_2O$, Riedel-de Haën, 99%) was dissolved in 100 ml of distilled water. These two solutions were mixed and stirred by magnetic stirrer. Then, 6.8 mmol of CTAB was added to the stirred solution. The Stirring takes place at $50^\circ C$ till it becomes colourless and clear. Then, the mixture was left to reach room temperature. In another flask, 1 mmol of Sodium sulfide 9-hydrate ($Na_2S \cdot 9H_2O$, Riedel-de Haën, 60-62%) was dissolved in 100 ml of distilled water, and then added to the former solution, drop by drop, under stirring at room temperature. During the reaction, changes in the colour of solution were observed. The colour changes from colourless to yellow orange for CdS. The strength of yellow orange colour decreases as Zn content increases and then becomes yellow white for ZnS. Then, the precipitate was left in the reaction vessel for 5 days. The precipitate was separated by centrifugation, washed several times with distilled water to remove residual impurities and then dried at $80^\circ C$. Thus, $Cd_{1-x}Zn_xS$ powder was produced and grinded into fine powder using an agate mortar. The chemical reaction of sample formation occurs as follows:



The powder was used to record EDX and XRD spectra. For HRTEM measurements a drop of diluted colloidal solution was deposited on 200 mesh copper grid coated with carbon and left to evaporate at room temperature forming a layer of nanoparticles.

2.2 Structural Characterization

The elemental compositions of the prepared samples were investigated by Oxford link ISIS electron dispersion X-ray with scanning electron microscope (JEOL JSM-5400) operating at an accelerating voltage of 30 keV. The structural characterization of $Cd_{1-x}Zn_xS$ nanopowders was performed by Shimadzu XRD-6000 diffractometer operated at voltage 40 kV and current 30 mA. The radiation source used was monochro-

matic CuK α 1 radiation ($\lambda = 0.15406$ nm) with scan speed of 2 ° per minute and scanning angular range from 4° to 80°. High resolution transmission electron micrograph (HRTEM) and selective area electron diffraction (SAED) patterns were taken by using JEOL® JEM-2100LaB6 HRTEM operating at an accelerating voltage of 200 kV and equipped with 4 mega pixel Gatan® CCD camera (Orius SC200B). UV-vis absorption spectra were collected with Lambda 45, Perkin, England. 10 mgm of each sample is dissolved in 25 ml of distilled water by using magnetic stirrer for UV-vis investigations.

3. RESULTS AND DISCUSSION

3.1 Energy Dispersive X-ray

The elemental compositions of Cd_{1-x}Zn_xS nanopowder with different Zn content were investigated by the energy dispersive x-ray analysis. Figure 1 shows a representative EDX spectrum of Cd_{0.5}Zn_{0.5}S at room temperature indicating clearly that the product contains Cd, Zn and S with no significant impurities. Table 1 represents the quantitative analysis of the measured composition ratio Cd: Zn: S as well as the initial compositions. In the present work the compositions will be denoted as the initial ones for convenience's sake, although the measured concentrations are as presented in table 1. Elemental compositional deviations for the present system have been previously reported [1, 29].

3.2 X-ray diffraction

X-ray diffraction yields information about crystalline structure and crystalline size. Figure 2 shows the XRD patterns of Cd_{1-x}Zn_xS nanopowder with different Zn content. The diffraction spectra are obtained by scanning the diffracting angles, 2θ , in the range from 10° to 80° at room temperature. The XRD pattern of CdS sample shows three prominent peaks that could be indexed to the diffraction from (111), (220) and (311) lattice planes of cubical zinc blend structure (ICCD- card no: 89-0440), respectively. The characteristic XRD peaks of ZnS of Fig. 2 could also be considered as (111), (220) and (311) lattice planes diffraction of cubical zinc blend structure (ICCD card No. 05-0566), respectively. Compared with CdS samples, the

other investigated samples with different Zn content have the same characteristic peaks. Based on this, it could be concluded that all the as-prepared samples have the same zinc blend structure, in agreement with the reported results of Jana et al [30] and Zhu et al [1]. It is also noticed that the diffraction peaks systematically shift to higher diffraction angle side from CdS to ZnS with the increasing of Zn content. The gradual peak shifting of the investigated samples provides good evidence for true solid solution formation of Cd_{1-x}Zn_xS and not a mixture of CdS and ZnS, in agreement with the reported data of refs. [1, 11] At this point it should be noted that there are shoulders around 25 and 28° and a low intensity peak is observed at 48° in the XRD spectra of Cd_{1-x}Zn_xS nanoparticles except for ZnS. These are corresponding to the hexagonal phase (JPCD 01-0783, 77-2306 and 01-0783) in the XRD spectra, respectively. As it can be seen from the XRD spectra, the percentage of the hexagonal phase is insignificant compared with the cubical zinc blend structure and gradually decreases with the increase of Zn content.

The interplaner lattice spacings, d , were calculated from the peak position using Bragg's equation

$$d = \lambda / (2 \sin \theta)$$

where λ is the wavelength of the X-ray used. The change of d and 2θ for various diffraction planes with different Zn content for Cd_{1-x}Zn_xS samples along with the corresponding values from the ICCD cards are listed in table 2. A systematic decrease in d is observed as the content of Zn increases and the magnitude of 2θ increases with the increase of Zn content in agreement with the reported results of ref. [31]. In case of the cubical zinc blend structure, the lattice constant, a , is calculated using the following expression:

$$1/d^2 = (h^2 + k^2 + l^2) / a^2$$

The calculated lattice constants for ZnS and CdS are 0.541 nm and 0.583 nm, respectively. These are in agreement with previous reported data [20, 31]. Figure 3 shows a relation between the lattices constant and the Zn content, which is nearly linear relationship. This trend is consist-

ent with Vegard's law, revealing a homogenous alloy structure [12]. The gradual decrease in the cell constant with increasing Zn content suggests that the increase in the concentration of Zn might introduce a strain in the samples that leads to decrease in the volume of the lattice and consequently decrease in the lattice constant. The ionic radius of Zn^{2+} (0.74 Å) is smaller than the ionic radius of Cd^{2+} (0.97 Å) and thus Zn ions might be incorporated into the CdS lattice or entered its interstitial sites [11]. Debye-Scherrer formula [22] was applied to calculate the crystallite sizes of the investigated samples

$$D = 0.9\lambda/\beta \cos\theta$$

Here D is the coherent length, β is the full-width at half-maximum (FWHM) of the peak in radians, and θ is the angle of diffraction. In single-crystal samples, crystallite size corresponds to particle size while in polycrystalline sample they differ [20]. In the case of spherical crystallites, the relation between D and the diameter of crystallite r, is given by [22]

$$D = (3/4)r$$

The corresponding crystallite sizes of nanoparticles obtained in this way are listed in table 2. This shows that the crystallite size decreases with increasing Zn content, in agreement with the previous work of ref. [31].

3.3 High Resolution Transmission Electron Microscopy

Transmission electron microscopy is used to identify the morphology, the size and the crystallographic structure of nanoparticles. Figures 4(a)- 8(a) represent the TEM micrograph of $Cd_{1-x}Zn_xS$ nanoparticles with different Zn content. As shown in these figures all $Cd_{1-x}Zn_xS$ nanoparticles have the same morphology of nearly nanospheres (QDs). The selected area electron diffraction, SAED, (the inset) show set of rings with spots corresponding to diffraction from different planes of the nanoparticles. SAED pattern shows three rings, which correspond to (111), (220) and (311) lattice plane of cubic phase of CdS (Fig 4 (a)). SAED patterns of the other four compositions show similar set of rings which supports the formation of cubic phase by showing (111), (220) and (311) lattice planes. The correspond-

ing lattice spacings are listed in table 3 along with those estimated from XRD for comparison. From this table it is clear that the d values obtained from HRTEM are in agreement with XRD measurement. The obtained set of rings indicates that all the as synthesized nanoparticles are polycrystalline in nature in agreement with XRD results. An overview of the TEM images illustrated in fig. 4 (a) - 8 (a) show that the size of nanoparticles of $Cd_{1-x}Zn_xS$ is decreasing with increasing Zn content except for ZnS. This is consistent with the XRD measurements. The mean particle sizes are estimated to be about 10 ± 1 , 9 ± 0.7 , 8.5 ± 0.8 , 7 ± 0.5 and 9 ± 1.1 nm for $Cd_{1-x}Zn_xS$ ($x = 0, 0.2, 0.5, 0.7$ and 1 , respectively). These sizes are larger than the sizes derived from Debye-Scherrer formula. The unexpected large particle size for ZnS might be due to the agglomeration of fine particles that are noticed from Fig. 8 (a). Figures 4(b)- 8(b) show the HRTEM images of the investigated samples. Lattice planes are visible in these images. Measurement of the interplaner spacing suggests that these parallel lattice planes are from (111) and (220) planes of cubic $Cd_{1-x}Zn_xS$ phase. The corresponding lattice spacings are presented in table 3.

3.4 Optical Properties

Figure 9 a-b shows the room temperature UV-vis absorption spectra of $Cd_{1-x}Zn_xS$ QDs with different Zn content ($0 \leq x \leq 1$) in the wavelength range from 300 to 700 nm. The spectra exhibit absorption edges at 485, 443, 425, 343 and 325 nm of $Cd_{1-x}Zn_xS$ nanoparticles ($x = 0, 0.2, 0.5, 0.7, 1$) respectively, which show blue-shift systematically with the increasing of Zn content. The band gap energies of $Cd_{1-x}Zn_xS$ nanoparticles were determined by the following equation [32]

$$\alpha h\nu = A(h\nu - E_g)^n$$

where α is the absorption coefficient, E_g is the absorption band gap energy, A is a constant and n is a parameter depends on the type of transition, n may have values 1/2, 2, 3/2 and 3 corresponding to allowed direct, allowed indirect, forbidden direct and forbidden indirect transitions respectively. The dependence of $(\alpha h\nu)^{1/n}$ on the photon energy $h\nu$ was plotted for different values of n. The best fit was found to be with $n = 1/2$. This is

a characteristic behavior of direct allowed transition. Figure 10 shows the graphs of $(\alpha h\nu)^2$ against $h\nu$ for Cd_{1-x}Zn_xS nanocrystals with different Zn content. The extrapolation of absorption curve $(\alpha h\nu)^2$ versus $h\nu$ to the value $(\alpha h\nu)^2$ equal zero yields the value of E_g . The variation of band gap energies with Zn Content for Cd_{1-x}Zn_xS nanoparticles is presented in Fig 11. The blue shifts relative to the bulk values of E_g for CdS and ZnS are found to be 0.18 eV and 0.44 eV, respectively. This observed enhancement of optical band gaps are known to arise from quantum-size-confinement effect in the UV- visible absorption. Jana and Coworkers [31] and Zhu and Coworkers [1] previously reported the blue shifts in Cd_{1-x}Zn_xS nanocrystals. The blue shifts for CdS and ZnS films that have been reported in ref. [31] were 1.4 eV and 0.5 eV with particle sizes of about 3 nm and 5 nm measured from TEM, respectively. On the other hand Zhu et al [1] reported blue shifts of 0.69 eV and 0.88 eV for CdS and ZnS nanocrystals, respectively. The mean particle size for CdS [1] was about 4 nm that was measured from TEM. Here, it should be pointed out that the sizes of the blue shifts in our work are quantitatively lower than those of the previously reported data [1, 31]. This is might be due to larger nanoparticle sizes and stoichiometry deviation in our work. Also, nanoparticle sizes in the present work for CdS and ZnS nanocrystals are larger than the corresponding Bohr radius of excitons. Therefore lower values of blue shifts in the present work are expected.

Bruse derived the effective mass approximation formula to explain the blue shift [20]. This formula is given by

$$E_g^{nano} = E_g^{bulk} + \frac{h^2}{8r^2} \left\{ \frac{1}{m_e^*} + \frac{1}{m_h^*} \right\} - \frac{1.8e^2}{4\pi\epsilon\epsilon_0 r}$$

where E_g^{nano} is the band gap of the nanoparticle, E_g^{bulk} is the bulk semiconductor band gap, r is the radius of the nanoparticle, m_e^* is the effective mass of electron, m_h^* is the effective mass of hole, e is the charge of an electron, ϵ is the dielectric constant of the material and ϵ_0 is the vacuum permittivity constant. The second term is the quantum confinement of electron and

hole which lead to the blue shift, while the third term is the coulomb interaction energy between the hole and the electron. The crystallite sizes for Cd_{1-x}Zn_xS were calculated using Bruse formulation. The electronic parameters used for ZnS are: $E_g = 3.66$ eV, $\epsilon = 5.2$, $m_e = 0.4m_0$ and $m_h = 0.61m_0$ [1] and for CdS are: $E_g = 2.42$ eV, $\epsilon = 5.7$, $m_e = 0.19m_0$ and $m_h = 0.8m_0$ [20]. For the rest of the investigated samples, we have assumed that the effective mass of electron and hole linearly depend on the relative composition [12]. The corresponding bulk gap energies of Cd_{1-x}Zn_xS ($0.2 \leq x \leq 0.7$) are estimated by using the empirical relationship $E_g(x) = 2.42 + 0.9x + 0.3x^2$ [31] Figure 12 illustrated the particle sizes estimated from optical band shift with Zn content. As it can be noticed from this figure, the particle sizes decrease with the increase of Zn content in agreement with XRD and HRTEM results.

3.5 Thermal annealing effect on Cd_{1-x}Zn_xS nanoparticles

3.5.1. X-Ray Diffraction analysis

The investigated Cd_{1-x}Zn_xS nanoparticles were subjected to annealing at temperatures of 200, 250, 300, 350 and 400 °C for 2 hours and then allowed to cool to room temperature in the oven. The XRD patterns of the annealed compositions of Cd_{1-x}Zn_xS ($0 \leq x \leq 1$) are presented in figures 13- 17, respectively. It is apparent that, almost no change in the diffraction peak positions with increasing annealing temperatures of all samples. The overview of the XRD patterns of all samples showed that the annealing compositions have the same structure as the as prepared samples, whereas the annealed ZnS sample revealed additional three low intensity peaks. These peaks are observed around 32.9°, 69.5° and 76.8° which were indexed to (200), (400) and (331) lattice planes of cubical zinc blend structure (ICCD 05-0566). As it is seen from Figs. 13- 17 the percentage of the hexagonal phase decreases as the Zn content increases. Also, tendency for phase transformation, from cubic to hexagonal, upon annealing is clearly observed for all the investigated composition except for ZnS. The intensities of the peaks in the XRD spectra of all samples were found to be enhanced with the increase of the annealing temperatures.

Table 1 Elemental Compositions of Cd_{1-x}Zn_xS nanopowder

Initial composition	Measured composition
CdS	Cd _{1.1} S _{0.9}
Cd _{0.8} Zn _{0.2} S	Cd _{0.8} Zn _{0.3} S _{0.9}
Cd _{0.5} Zn _{0.5} S	Cd _{0.4} Zn _{0.7} S _{0.9}
Cd _{0.3} Zn _{0.7} S	Cd _{0.3} Zn _{0.9} S _{0.8}
ZnS	Zn _{1.1} S _{0.9}

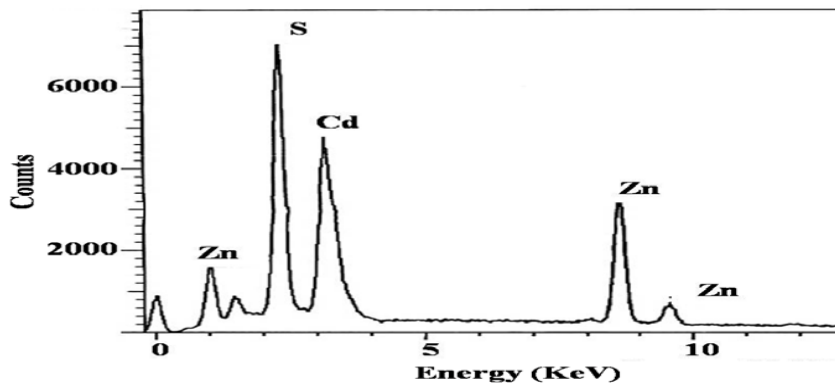


Figure 1

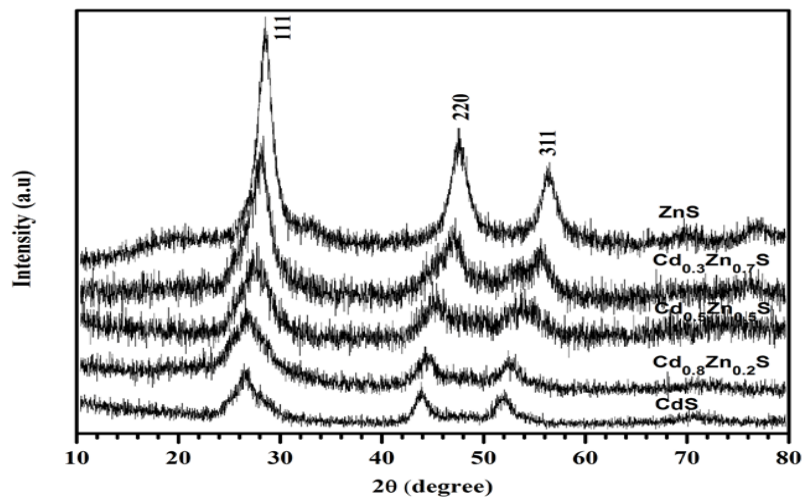


Figure 2

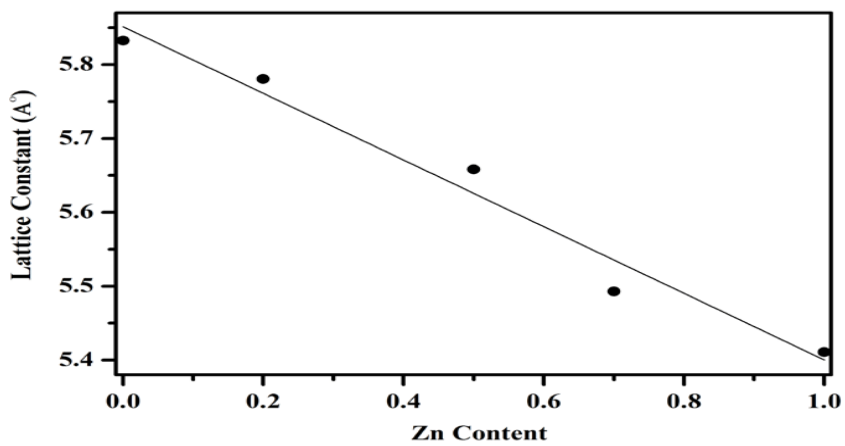


Figure 3

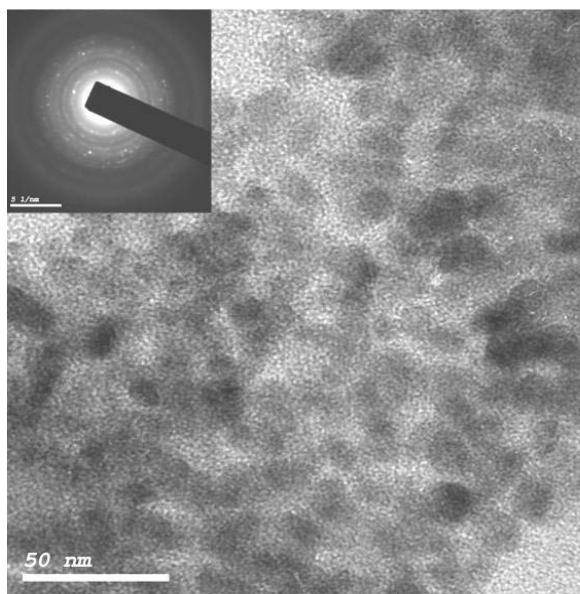


Figure 4- a

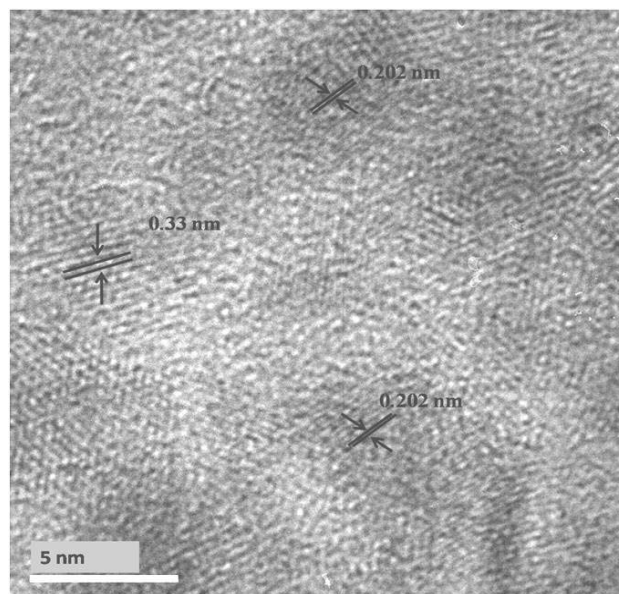


Figure 4- b

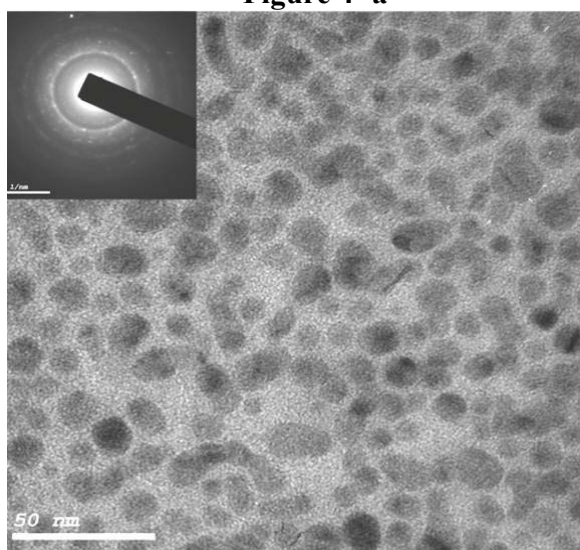


Figure 5- a

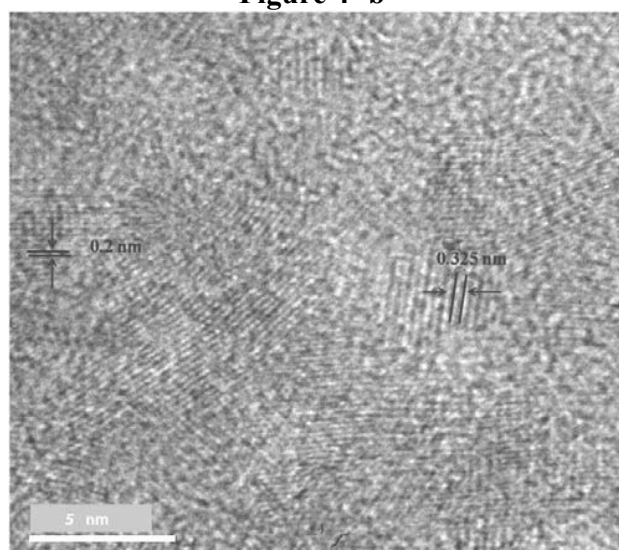


Figure 5- b

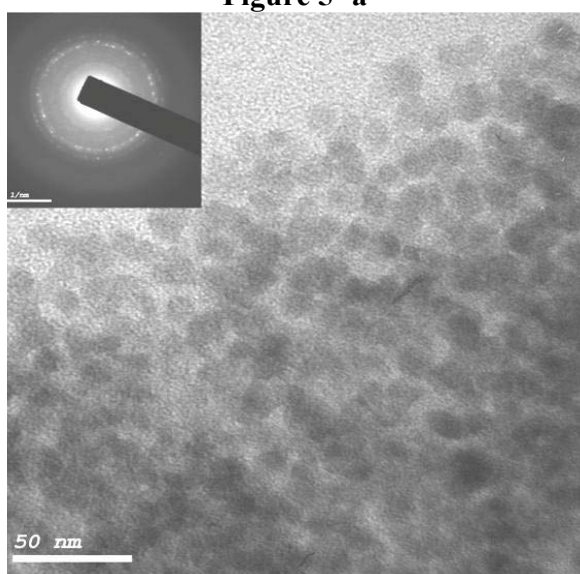


Figure 6- a

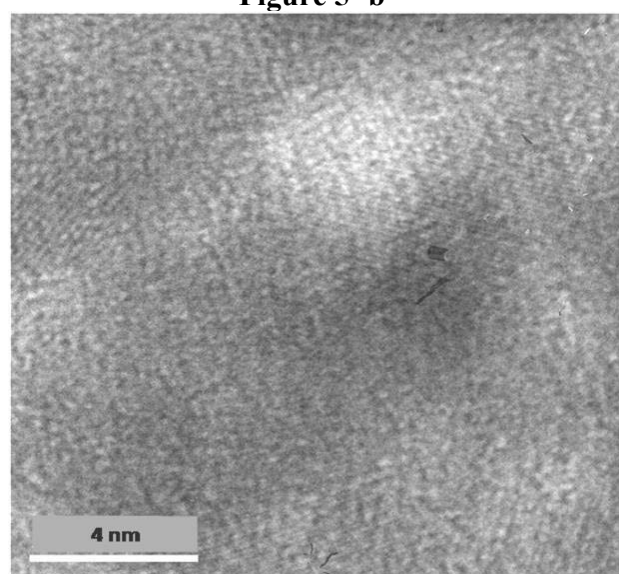


Figure 6- b

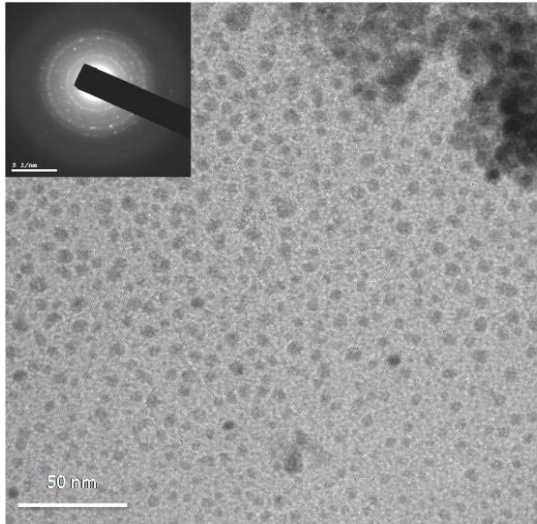


Figure 7- a

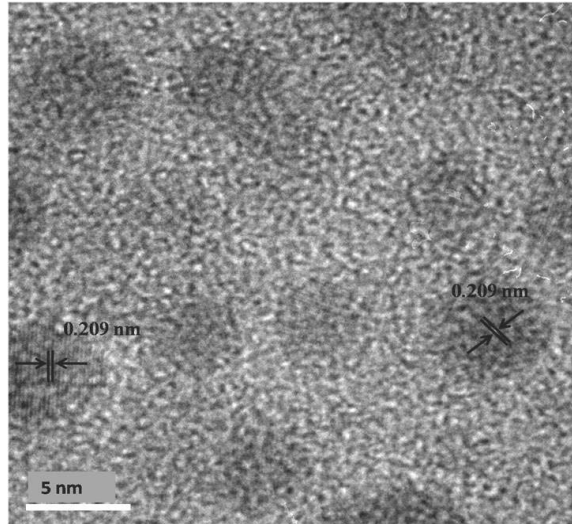


Figure 7- b

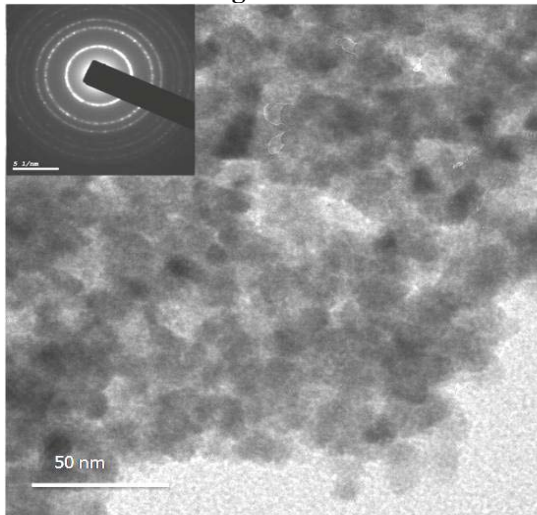


Figure 8- a

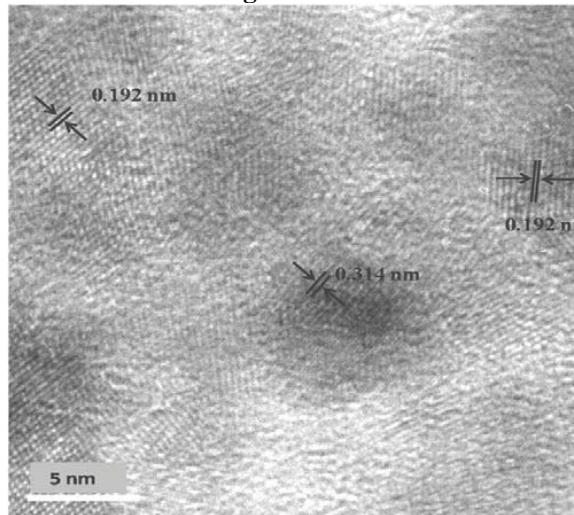


Figure 8- b

Table 2 Structural data of Cd_{1-x}Zn_xS nanocrystals from XRD along with those corresponding to ICDD cards

Sample	Experimental XRD data				ICDD cards			
	2θ (degree)	Intensity %	d (Å)	r* (nm)	2θ (degree)	d (Å)	(hkl)	ICDD card No.
CdS	26.52	100	3.358	6.4± 0.1	26.45	3.366	111	89-0440
	43.84	66	2.063		43.88	2.061	220	
	51.84	56	1.762		51.97	1.757	331	
Cd _{0.8} Zn _{0.2} S	26.78	100	3.326	5.6± 0.1	26.49			
	44.39	46	2.038		44.02			
	52.14	37	1.752		52.26			
Cd _{0.5} Zn _{0.5} S	27.63	100	3.257	5.3± 0.2	27.1		111	Ref. [30]
	45.12	42	2.007		45.88		220	
	53.72	36	1.705		53.53		311	
Cd _{0.3} Zn _{0.7} S	27.94	100	3.19	5.1± 0.1	27.3			
	46.92	34	1.934		45.3			
	55.57	24	1.652		55			
ZnS	28.49	100	3.13	6.4± 0.1	28.55	3.123	111	05-0566
	47.55	45	1.91		47.51	1.912	220	
	56.38	30	1.63		56.28	1.633	331	

* r represents the nanoparticle size.

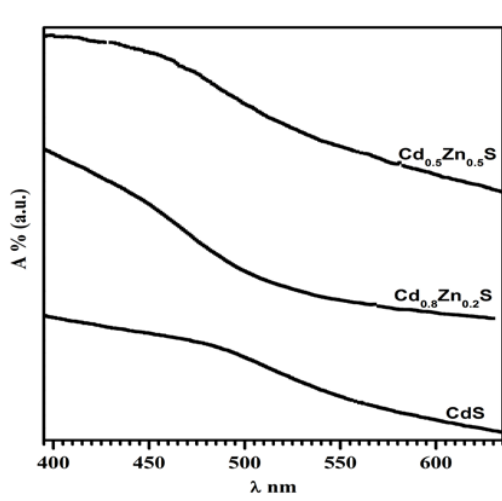


Figure 9- a

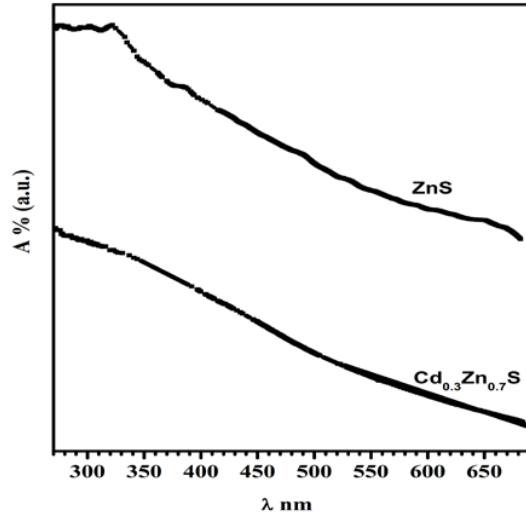


Figure 9- b

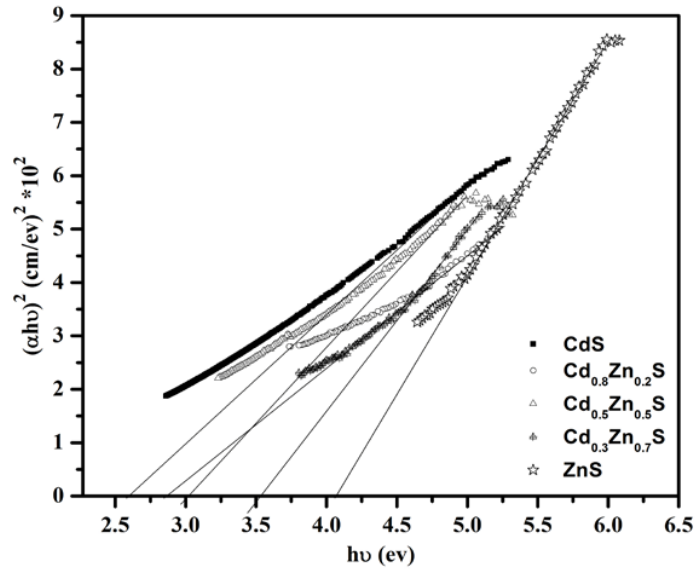


Figure 10

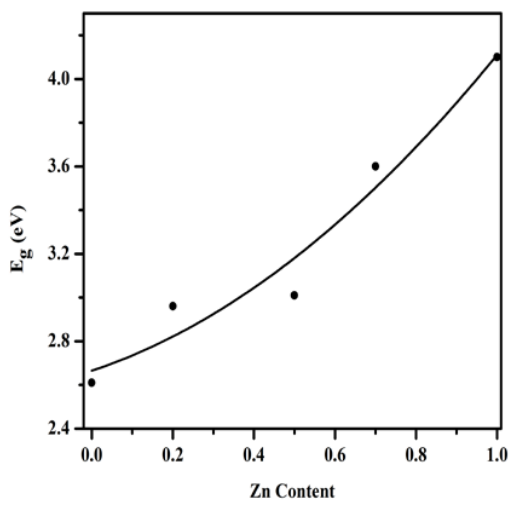


Figure 11

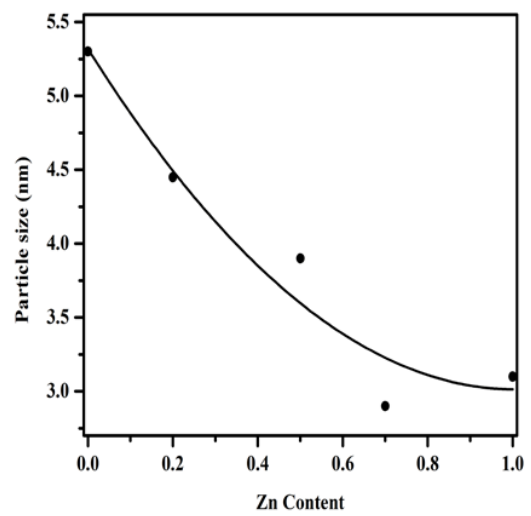


Figure 12

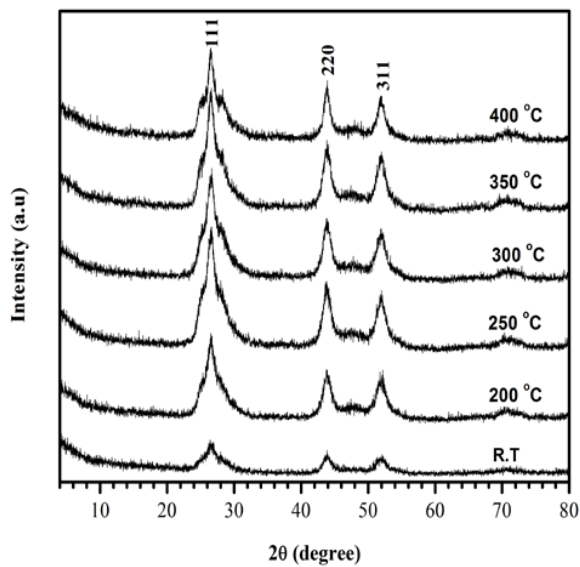


Figure 13

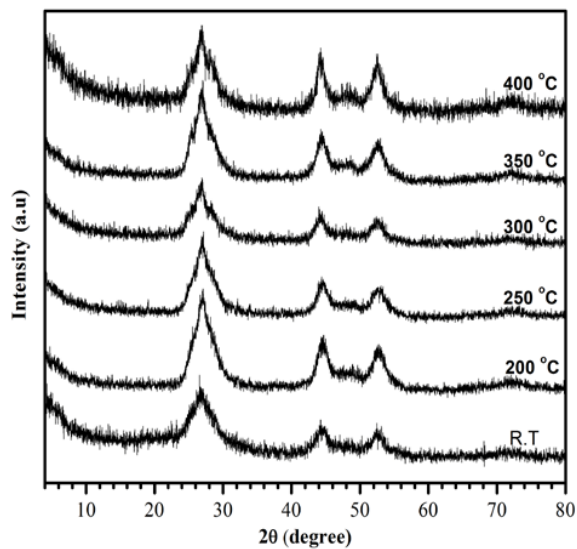


Figure 14

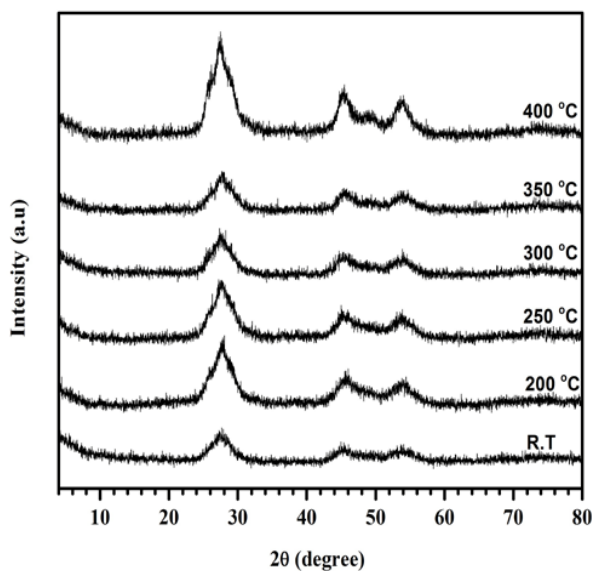


Figure 15

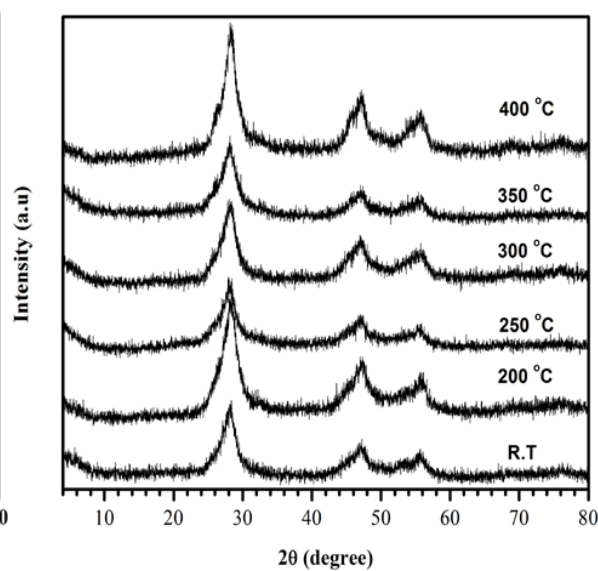


Figure 16

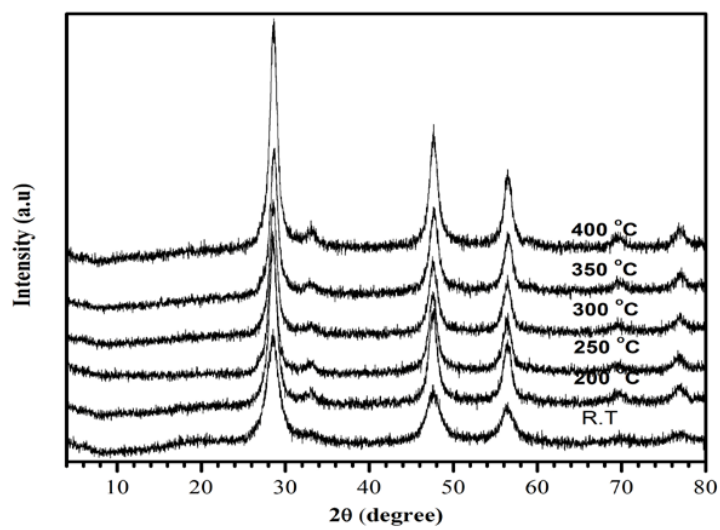


Figure 17

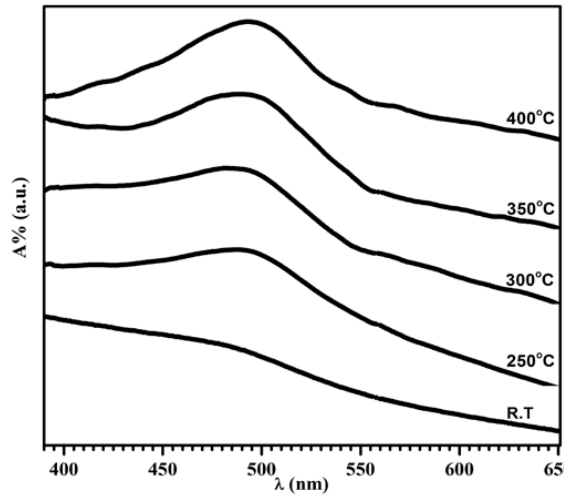


Figure 18

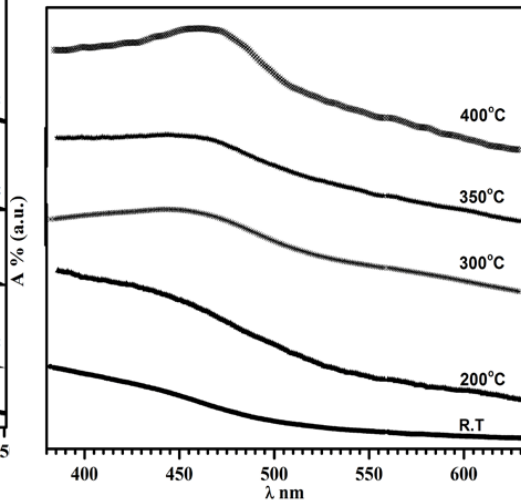


Figure 19

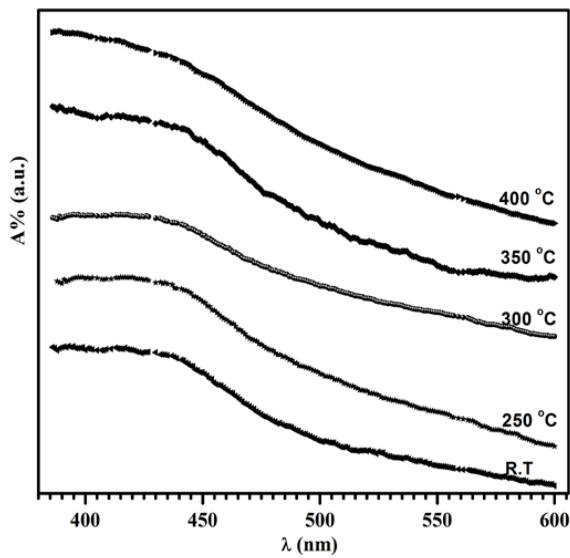


Figure 20

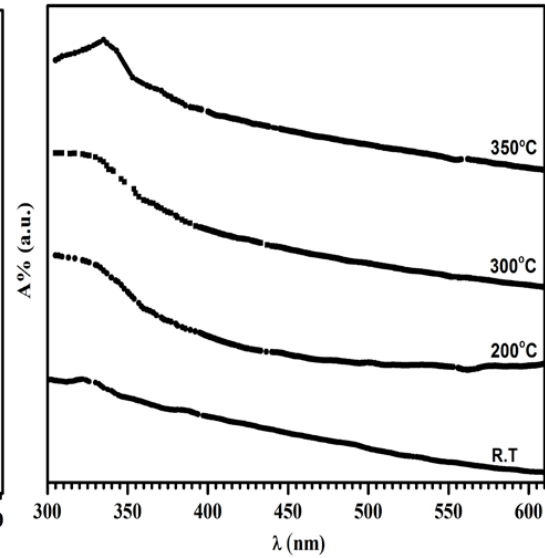


Figure 21

Table 3 Lattice spacings estimated from HRTEM and XRD

Sample	TEM	HRTEM	XRD	h k l
	d (Å)	d (Å)	d (Å)	
CdS	3.32	3.3	3.358	111
	2.04	2.02	2.063	220
	1.73	-	1.762	311
Cd _{0.8} Zn _{0.2} S	3.31	3.25	3.326	
	2	-	2.038	
	1.72	-	1.752	
Cd _{0.5} Zn _{0.5} S	3.22		3.257	111
	1.98		2.007	220
	1.69		1.705	311
Cd _{0.3} Zn _{0.7} S	3.15	-	3.19	
	1.92	1.95	1.934	
	1.62	-	1.652	
ZnS	3.08	3.14	3.13	111
	1.90	1.92	1.91	220
	1.61		1.63	311

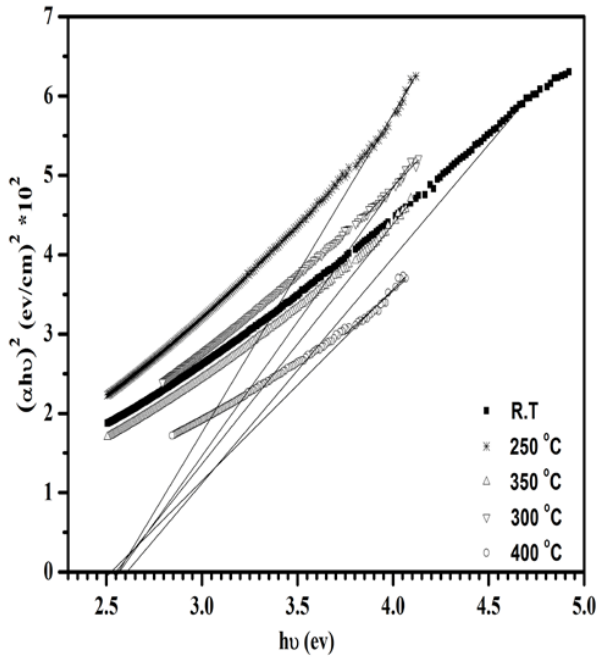


Figure 22

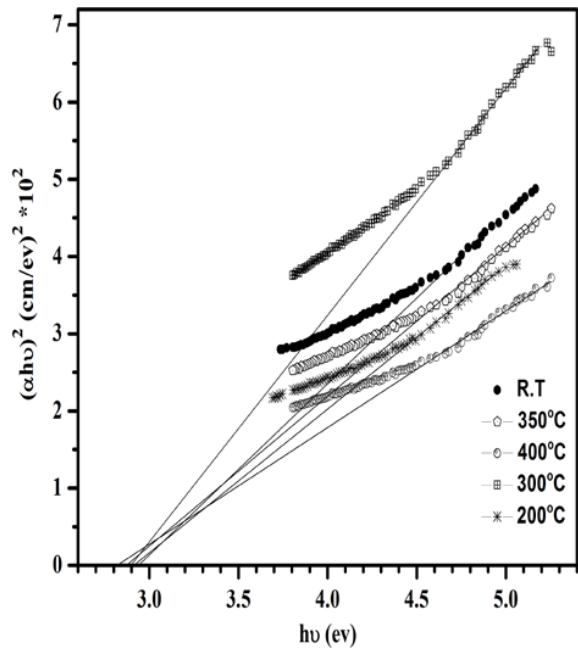


Figure 23

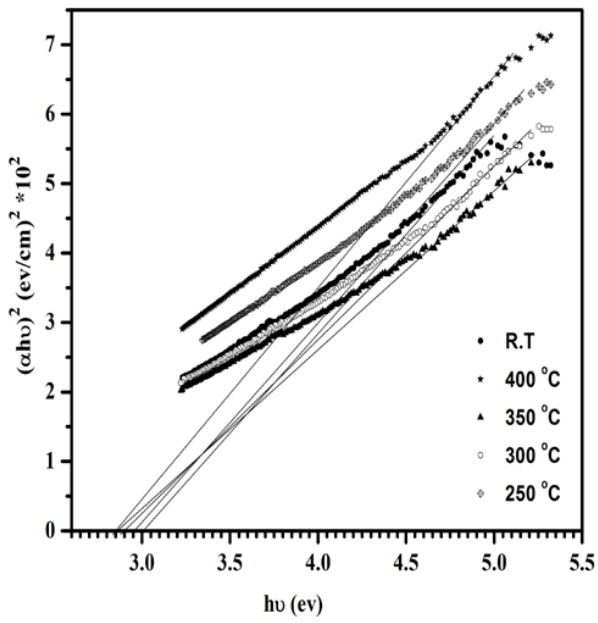


Figure 24

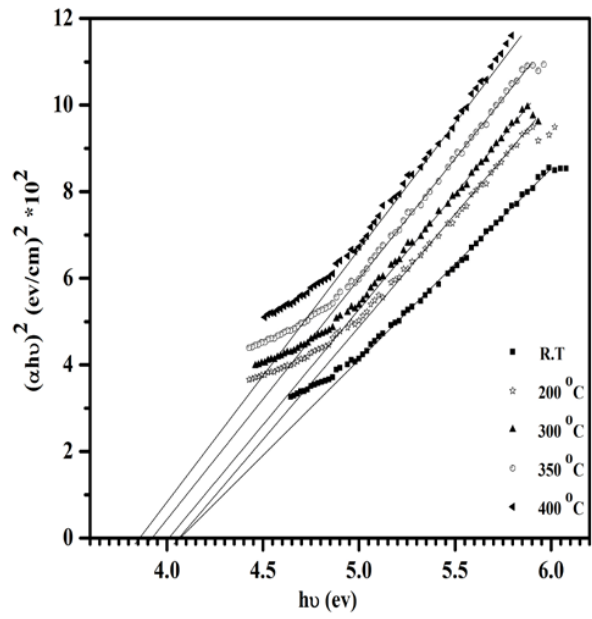


Figure 25

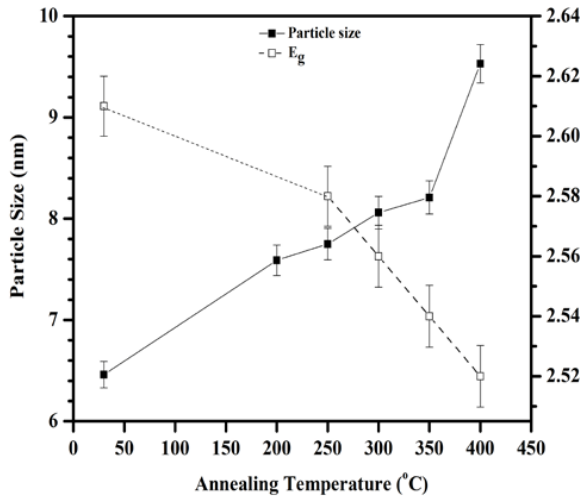


Figure 26

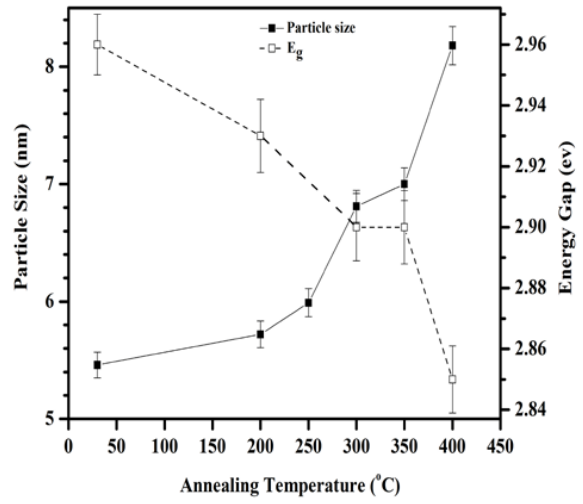


Figure 27

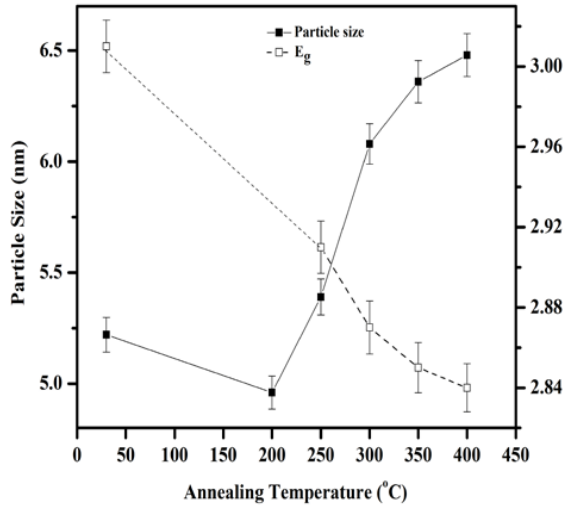


Figure 28

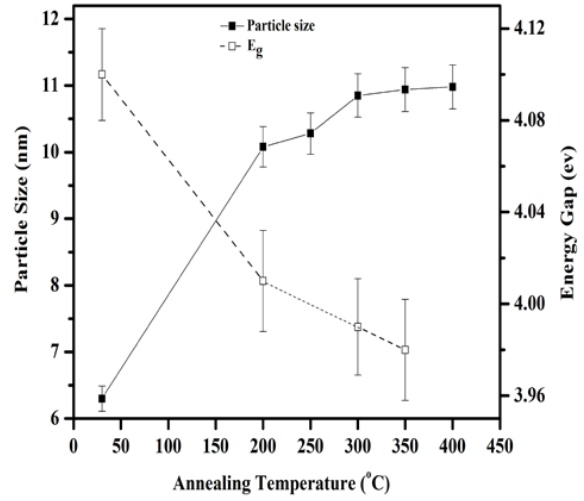


Figure 29

List of Figures

Figure 1 EDX spectra of $\text{Cd}_{0.5}\text{Zn}_{0.5}\text{S}$ nanoparticles

Figure 2 XRD patterns of $\text{Cd}_{1-x}\text{Zn}_x\text{S}$ nanoparticles at room temperature

Figure 3 A plot between the lattice constant and Zn content

Figure 4 (a): TEM and (b) HRTEM images of CdS nanoparticles

Figure 5 (a): TEM and (b) HRTEM images of $\text{Cd}_{0.8}\text{Zn}_{0.2}\text{S}$ nanoparticles

Figure 6 (a): TEM and (b) HRTEM images of $\text{Cd}_{0.5}\text{Zn}_{0.5}\text{S}$ nanoparticles

Figure 7 (a): TEM and (b) HRTEM images of $\text{Cd}_{0.3}\text{Zn}_{0.7}\text{S}$ nanoparticles

Figure 8 (a): TEM and (b) HRTEM images of ZnS nanoparticles

Figure 9 Plot of UV-visible spectrum of $\text{Cd}_{1-x}\text{Zn}_x\text{S}$ nanoparticles at room temperature, (a) $x=0$, 0.2 and 0.5 and (b) $x=0.7$ and 1

Figure 10 Plot of $(\alpha h\nu)^2$ against $h\nu$ for $\text{Cd}_{1-x}\text{Zn}_x\text{S}$ nanoparticles at room temperature

Figure 11 The variation of band gap energies with Zn Content for $\text{Cd}_{1-x}\text{Zn}_x\text{S}$ nanoparticles

Figure 12 The variation of the particle sizes estimated from optical band shift with Zn content

Figure 13 XRD pattern for CdS nanoparticles at different annealing temperatures

Figure 14 XRD pattern for $\text{Cd}_{0.8}\text{Zn}_{0.2}\text{S}$ nanoparticles at different annealing temperatures

Figure 15 XRD pattern for $\text{Cd}_{0.5}\text{Zn}_{0.5}\text{S}$ nanoparticles at different annealing temperatures

Figure 16 XRD pattern for $\text{Cd}_{0.3}\text{Zn}_{0.7}\text{S}$ nanoparticles at different annealing temperatures

Figure 17 XRD pattern for ZnS nanoparticles at different annealing temperatures

Figure 18 Plot of UV-visible spectrum of CdS nanoparticles at different annealing temperatures

Figure 19 Plot of UV-visible spectrum of $\text{Cd}_{0.8}\text{Zn}_{0.2}\text{S}$ nanoparticles at different annealing temperatures

Figure 20 Plot of UV-visible spectrum of $\text{Cd}_{0.5}\text{Zn}_{0.5}\text{S}$ nanoparticles at different annealing temperatures

Figure 21 Plot of UV-visible spectrum of ZnS nanoparticles at different annealing temperatures

Figure 22 Plot of $(\alpha h\nu)^2$ against $h\nu$ for CdS nanoparticle at at different annealing temperatures

Figure 23 Plot of $(\alpha h\nu)^2$ against $h\nu$ for $\text{Cd}_{0.8}\text{Zn}_{0.2}\text{S}$ nanoparticle at at different annealing temperatures

Figure 24 Plot of $(\alpha h\nu)^2$ against $h\nu$ for $\text{Cd}_{0.5}\text{Zn}_{0.5}\text{S}$ nanoparticle at at different annealing temperatures

Figure 25 Plot of $(\alpha h\nu)^2$ against $h\nu$ for ZnS nanoparticle at at different annealing temperatures

Figure 26 The variation of E_g and the particle size at different annealing temperatures of CdS

Figure 27 The variation of E_g and the particle size at different annealing temperatures of $\text{Cd}_{0.8}\text{Zn}_{0.2}\text{S}$

Figure 28 The variation of E_g and the particle size at different annealing temperatures of $\text{Cd}_{0.5}\text{Zn}_{0.5}\text{S}$

Figure 29 The variation of E_g and the particle size at different annealing temperatures of ZnS

This indicates that the crystallinity of the studied samples improved after annealing. The particle sizes were derived from Debye-Scherrer formula [22]. It was found that the particle size increases with increasing the annealing temperature. The increased particle sizes after annealing could be due to improving crystallinity as a result of heat treatment. The increase in particle size after annealing might affect the sizes of the band gaps of the investigated samples. Therefore, it was instructive to look at the size of band gap upon annealing.

3.5.2 Optical properties of the annealed samples

Figures 18 - 21 show the UV-visible absorption spectra of Cd_{1-x}Zn_xS nanoparticles at different annealing temperatures in the range 290- 700 nm. The spectra exhibit absorption edges which show a red-shift with the increase of annealing temperatures. Figures 22-25 show graphs of $(\alpha h\nu)^2$ against $h\nu$ for Cd_{1-x}Zn_xS nanocrystals with different Zn content at different annealing temperatures. The estimated band gap energies, from these graphs, showed decrease with increasing annealing temperature. The variation of E_g and particle size, estimated from XRD studies, at different annealing temperatures for all studied samples are illustrated in figures 26-29. The decreased band gap after annealing could be caused by the increase of particle size upon annealing. It was noticed that the decreased percentage in E_g is about 2 - 5%, whereas the corresponding increased percentage in particle size, estimated from XRD, upon annealing was about 25 – 74%. This indicates that the extent at which particle size changes with annealing is much higher than the corresponding change in E_g .

CONCLUSION

Cd_{1-x}Zn_xS quantum dots have been prepared by coprecipitation method using CTAB as a capping agent. XRD investigations revealed that the as-synthesized samples are polycrystalline having a mixture of cubic and hexagonal phases. The hexagonal phase has a very small percentage and decreased till it goes to zero as x increased from 0 to 1. The lattice constant decreased with the increase of Zn content. This provided evidence for the formation of a homogeneous al-

loy structure. Also, the particle size decreased with increasing Zn content. HRTEM showed the presence of quantum dots and confirmed the XRD results. UV- vis absorption studies showed a blue shift in the optical band edges relative to the corresponding bulk materials as an indication to quantum confinement effect. The band gap energy increased gradually with the increase of Zn content. The particle size, estimated from Brus equation, showed a decrease with the increase of Zn content which is consistent with the trend observed in the XRD and HRTEM results. Studies of XRD under different annealing temperature showed that the annealed compositions have the same structure as the as-synthesized samples. The annealed ZnS revealed additional three low intensity peaks which were indexed to (200), (400) and (331) of cubical zinc blend structure. The percentage of the hexagonal phase decreased as the Zn content increased. Tendency for phase transformation from cubic to hexagonal upon annealing was also, observed. In addition, the XRD studies revealed an improvement in the crystallinity of the material after heat treatment. The particle size increased with the increase of the annealing temperature. UV- vis absorption investigations showed red shift in the optical band edge relative to the as-synthesized samples with annealing. The optical band gap decreased after annealing which might have been due to an increase in the particle size upon annealing. Thus, the optical properties of Cd_{1-x}Zn_xS nanomaterials can be tuned as required by thermally annealing it or varying the relative ratio of Cd and Zn for specific practical application.

REFERENCES

1. J. Zhu, J. Zhen, C. Chen, J. Lu and S. Chen, J. Physica B, "Controllable Synthesis of Water-Soluble Luminescent Cd_xZn_{1-x}S Nanocrystals", Vol. 405, 2010, pp. 3452–3457.
2. R. Viswanatha and D.D. Sarma, "Nanomaterials Chemistry: Recent Developments and New Directions", Chapter 4, Wiley-VCH, Germany, 2007.
3. H. Weller, J. Phys. Eng. Sci. "Synthesis and self-assembly of colloidal nanoparticles", Vol. 361, Iss. 1803, 2003, pp. 229–240.
4. L.E. Brus, J. Appl. Phys. A: Mater. Sci. Surfaces, "Quantum Crystallites and Nonlinear Optics", Vol. 53, 1991, pp. 465–474.
5. R.A.M. Hikmet, V. Talapin and H. Weller, J. Appl. Phys., "Study of Conduction Mechanism and Electro-

- luminescence in CdSe/ZnS Quantum Dot Composites“, Vol. 93, 2003, pp.3509–3514.
- S.Y. Kim, D.S. Kim, B.T. Ahn and H.B. Im, *J. Mater. Sci. Mater. Electronics*, “Electrical and Optical Properties of Vacuum-evaporated CdS Films“, Vol. 4, 1993, pp. 178- 182.
- T. P. Kumar, S. Saravanakumar and K. Sankaranarayanan, *J. Applied Surface Science*, “Effect of annealing on the surface and band gap alignment of CdZnS thin films“, Vol. 257, 2011, pp. 1923–1927.
- V. Kumar, S. K. Sharma and D.K. Dwivedi, *J. Alloys and Compounds* “Crystallographic, optical and electrical properties of low zinc content cadmium zinc sulphide composite thin films for photovoltaic applications“ Vol. 512, 2012, pp. 351– 354.
- N. A. Al-Tememe, N. M. Saeed, S. M. A. Al-Dujayli and B. T. Chiad, *J. Adv. Mater. Phys. Chem.*, “The Effect of Zn Concentration on the Optical Properties of Cd_{1-x}Zn_xS Films for Solar Cells Applications“, 2012, 2, 69-74
- L. S. Ravangave and U. V. Biradar, *IOSR J. Appl. Phys.*, “Study of structural, Morphological and Electrical Properties of Cd_xZn_{1-x}S Thin Films“, Vol. 3, Issue 3, 2013, pp. 41-47.
- S. Zu, Z. Wang, B. Liu, X. Fan and G. Qian, *J. Alloys Compd.*, “Synthesis of Nano- Cd_xZn_{1-x}S by Precipitate-hydrothermal Method and its Photocatalytic Activities“, Vol. 476, 200, pp. 689–692.
- L. Wang, Y. Jiang, C. Wang, W. Wang, B. Cao, M. Niu and Y. Qian, *Journal of Alloys and Compounds*, “Composition-controllable synthesis and optical properties of non-integral stoichiometry compound Zn_xCd_{1-x}S nanorods“, Vol. 454, 2008, pp. 255–260.
- D. V. Petrov, B. S. Santos, G. A. L. Pereira, and C. d. M. Donega, *J. Phys. Chem. B*, “Size and Band-Gap Dependences of the First Hyperpolarizability of Cd_xZn_{1-x}S Nanocrystals“, Vol. 106, 2002, 5325-5334.
- S. Saha, S.Sain, A.K.Meikap, S.K.Pradhan, *Physica E*, “Microstructure Characterization and Electrical Transport of Nanocrystalline CdZnS Quantum Dots“, Vol. 66, 2015, pp. 59–66.
- T. Yamaguchi, J. Matsufusa and A. Yoshida, *Jpn. J. Appl. Phys.* “Optical Transitions in RF Sputtered CuIn_xGa_{1-x}Se₂ Thin Films“, Vol. 31, 1992, L703.
- J.H. Lee, W.C. Song, J.S. Yi, K.J. Yang, W.D. Han and J. H wang, “ Growth and properties CuGaSe₂ thin films for solar cell applications“, vol. 431-432, (2003), pp. 349-353. *J. Thin Solid Films*, Vol. 349, 2003, pp. 431–432.
- K. Bando, T. Sawabe, K. Asaka and Y. Masumoto, *J. Luminescence*, “Room-temperature excitonic lasing from ZnO single nanobelts“ Vol. 108, 2004, p. 385.
- H. Kind, H. Yan, B. Messer, M. Law and P.D. Yang, *J. Adv. Mater.*, “Nanowire Ultraviolet Photodetectors and Optical Switches“ , Vol. 14, 2002, pp. 158-160.
- M. Salavati-Niasari, F. Davar and M. Mazaheri, *J. Alloys Compd Synthesis and characterization of ZnS nanoclusters via Hydrothermal Processing from [bis(salicylidene)zinc(II)]“*, Vol. 470, 2009, pp. 502–506.
- V. Singh and P. Chauhan, *J. Phys. and Chem. of Solids*, “Structural and Optical Characterization of CdS Nanoparticles Prepared by Chemical Precipitation Method“ Vol. 70, 2009, pp. 1074–1079.
- H.F. Shao, X. F. Qian and Zi. K. Zhu, *J. Solid State Chemistry*, “The synthesis of ZnS hollow nanospheres with nanoporous shell“ Vol. 178, 2005, pp. 3522–3528
- M. Behboudni and B. Khanbabaee, *J. Colloids and Surfaces A: Physicochem. Eng. Aspects*, “Conformational Study of CdS Nanoparticles Prepared by Ultrasonic Waves“, Vol. 290, 2006, pp. 229–232.
- T. Zhai, X. Zhang, W. Yang, Y. Ma, J. Wang, Z. Gu, D. Yu, H. Yang and J. Yao, *J. Chem. Phys. Lett.*, “Growth of single crystalline Zn_xCd_{1-x}S Nanocombs by Metallo-organic Chemical Vapor Deposition“, Vol. 427, 2006, pp. 371–374.
- M.F. Kotkata, A.E. Masoud, M.B. Mohamed and E.A. Mahmoud, *J. Chalcogenide Lett.*, “Effect of Aging Period on the Structural Characterization of Fresh and Thermally-annealed CdS Nanoparticles“ , Vol. 5, 2008, pp. 209- 217.
- M. Tan, W. Cai and Lide Zhang, *J. Appl. Phys. Lett.* “Optical absorption of ZnS nanocrystals inside pores of silica“ Vol. 71, 1997, pp. 3697.
- X. J. Xu, G. T. Fei, W. H. Yu, X. W. Wang, L. Chen and L. D. Zhang “Preparation and formation mechanism of ZnS semiconductor nanowires made by the electrochemical deposition method“ Vol. 17, 2006, pp. 426-429.
- S.K. Mandal, S. Chaudhuri and A.K. Pal, *J. Thin Solid Films*, “ Optical properties of nanocrystalline ZnS films prepared by high pressure magnetron sputtering“, Vol. 350, 1999, pp. 209-213.
- B Bhattacharjee, S K Mandal, K Chakrabarti, D Ganguli and S Chaudhuri, *J. Phys. D: Appl. Phys.* “Optical properties of Cd_{1-x}Zn_xS nanocrystallites in sol–gel silica matrix“ Vol. 35, 2002, pp. 2636–2642.
- G.H. Yue, P.X. Yan , D. Yan, J.Z. Liu, D.M. Qu, Q. Yang and X.Y. Fan, *J. Crystal Growth Synthesis* of two-dimensional micron-sized single-crystalline ZnS thin nanosheets and their photoluminescence properties“, Vol 293, 2006, pp. 428–432.
- M.A. Rafea, A.A.M. Farag and N. Roushdy, *J. Alloys Compd*, “Structural and Optical Characteristics of Nano-sized Structure of Zn_{0.5}Cd_{0.5}S thin films prepared by Dip-coating Method“, Vol. 485, 2009, pp. 660–666.
- S. Jana, R. Maity, S. Das, M.K. Mitra and K.K. Chattopadhyay, *Physica E*, “Synthesis, Structural and Optical Characterization of Nanocrystalline Ternary Cd_{1-x}Zn_xS Thin Films by Chemical Process“, Vol. 39, 2007, pp. 109–114.
- J.I. Pankove, “Optical Processes in Semiconductors, Prentice-Hall“, Englewood Cliffs, NJ, 1971.